Spatially quasiperiodic convection and temporal chaos in two-layer thermocapillary instabilities

P. Colinet,[1] Ph. Géoris,[1] J. C. Legros,[1] and G. Lebon[2]
[1]*Microgravity Research Center, Université Libre de Bruxelles, CP 165, 50, av. F. D. Roosevelt, 1050 Bruxelles, Belgium*
[2]*Thermodynamique des Phénomènes Irréversibles, Université de Liège, Sart-Tilman, B-4000, Liège, Belgium*
(Received 7 December 1995)

This paper describes an amplitude equation analysis of the interactions between waves with wave number k_1 (and phase speed ω_c/k_1) and stationary convection with wave number k_2. These two modes may bifurcate almost simultaneously from the conductive state of a two-layer Bénard system, when the ratio of layer thicknesses is near a particular value (codimension-2 singularity). When $k_2 \neq 2k_1$ (nonresonant case) and the first bifurcation occurs for steady convection, a secondary bifurcation to a spatially quasiperiodic and time-periodic mixed mode is obtained when increasing the driving gradient. No stable small-amplitude solution exists when the Hopf bifurcation is the first one. The occurrence of either of these two possibilities depends on the thickness ratio. When $k_2 = 2k_1$ (resonant case), the system presents a much wider variety of dynamical behaviors, including quasiperiodic relaxation oscillations and temporal chaos. The discussion of the resonant system concentrates on a scenario of transition to chaos consisting of an infinite sequence of ''period-doubling'' homoclinic bifurcations of stable periodic orbits, for which the left-right symmetry of the convective system plays an essential role. For increasing constraint, a reverse cascade is observed, for which quadratic nonlinearities in the Ginzburg-Landau equations are shown to entirely determine the dynamics (cubic and higher-order terms may be neglected near the codimension-2 point). [S1063-651X(96)09207-0]

PACS number(s): 47.20.−k, 47.35.+i, 47.54.+r, 05.45.+b

INTRODUCTION

Weakly nonlinear studies of instability phenomena proceeding on the basis of amplitude equations are justified by a number of interesting theoretical issues [1]. First of all, the form of such equations is entirely determined by the symmetries obeyed by the physical system, which immediately suggests the possibility of comparing different pattern-forming systems, through the nature and stability properties of their solutions. Furthermore, the analysis of evolution equations for the amplitudes of some near-critical modes (Ginzburg-Landau equations) allows us to describe phenomena possessing an infinite number of degrees of freedom (such as the hydrodynamical system considered here below) in terms of low-dimensional dynamical systems. While it is occasionally possible to show that these amplitude equations can be derived from a potential function (implying the monotonic decrease of this potential until a local minimum), this is not the general case, such that amplitude equations can also be expected to display more complex behaviors in some circumstances. This, in turn, offers the possibility of understanding some features of turbulent behaviors observed in extended systems in terms of deterministic chaos of dynamical systems [2].

A fundamental step in deriving amplitude equations is the identification of the nature and symmetry properties of the near-critical modes obtained by the resolution of the linear stability problem. In this presentation, we consider the interaction of a monotonic (neutrally stable) mode with an oscillatory (overstable) mode, each possessing a finite and different wave number. This differs from the previously treated cases of the interaction of two neutrally stable modes with finite wave numbers in the ratio 1:2 [3], or in the ratio 1:1 [4], and of the interaction of a Hopf bifurcation with a zero wave number with a neutrally stable mode with finite wave number [5]. Another relevant case is the codimension-2 point (CTP) occurring in Rayleigh-Bénard convection in binary mixtures [6,7], although the basic wave numbers of the instabilities are expected to differ more strongly in the present analysis (in particular, the case of strong resonance 2:1 is also investigated). An interesting recent work of Fujimura and Renardy [8] on a similar two-layer Rayleigh-Bénard system also treats this 2:1 steady-Hopf resonance case. They obtain amplitude equations identical to those derived here below. Consequently, some of their conclusions have a general character and are directly applicable here (e.g., the existence and stability of a new kind of asymmetric mode). However, differences exist between the basic mechanisms of instability (their oscillatory mode is interfacial, while surface deformability is unimportant for modes considered here), leading to different dynamical behaviors (through differences in the numerical coefficients of the amplitude equations). Some of these differences are stressed later on in this work.

The system considered here, of which no explicit use is made before the analysis of Sec. II apart from general symmetry properties, is a two-dimensional (2D) Marangoni-Bénard system obtained by sandwiching two layers of immiscible fluids of infinite horizontal extent between two rigid conducting plates maintained at different temperatures. Several solutions exist for the nonlinear equations describing such a system, one of them being the rest conductive solution. This state can become unstable [9,10] when the imposed temperature difference is raised above a critical value, which reduces to a condition on the Marangoni number, as long as the interfacial tension variation with temperature is the only destabilizing mechanism involved. No buoyancy effect is considered, and the interface is assumed to be undeformable. For this system, a set of parameter values exists (most of them being fixed by the choice of liquids) for which

waves of wave number k_1 and linear frequency ω_c are simultaneously critical with steady convection of wave number k_2. Accordingly, the deviation of the fields (temperature and velocity) with respect to the diffusive solution will be written, at the lowest perturbative order, as a superposition of critical eigenmodes with complex amplitudes

$$\begin{aligned} U(x,z,t) = & a_1(t)\exp[i(k_1 x+\omega_c t)]U_1(z) \\ & + a_2(t)\exp[i(k_1 x-\omega_c t)]U_2(z) \\ & + a_3(t)\exp[ik_2 x]U_3(z)+\text{c.c.}, \end{aligned} \tag{1}$$

where $U_2(z)=\overline{U_1}(z)$ and $U_3(z)$ is real (the overbar denotes the complex conjugate), x and z are the coordinates, respectively, parallel and perpendicular to the plane of the layers, and t is the time. We now derive the form of amplitude equations for the left- and right-traveling wave amplitudes a_1 and a_2, and for the steady mode amplitude a_3. The analysis is restricted to nonzero values of k_1, k_2, and ω_c.

I. DERIVATION OF THE FORM OF AMPLITUDE EQUATIONS ON THE BASIS OF SYMMETRY PROPERTIES

The amplitude equations are first written in the general form

$$\frac{da_i}{dt}=F_i(a_1,a_2,a_3,\overline{a_1},\overline{a_2},\overline{a_3}), \quad i=1,2,3 \tag{2}$$

and expanded in Taylor series around the origin $a_1=a_2=a_3=0$ (where the functions F_i vanish). The following symmetry considerations are then used to simplify the resulting system: the physical setup is invariant with respect to the following.

(i) Time translations $t\to t+\Delta t$ (autonomous system): according to Eq. (1), this is equivalent to the requirement that amplitude equations (2) are invariant under the transformation $\{a_1,a_2,a_3\}\to\{a_1\exp[i\theta],a_2\exp[-i\theta],a_3\}$ for every θ.

(ii) Lateral translations $x\to x+\Delta x$: this implies that Eqs. (2) are invariant under the transformation $\{a_1,a_2,a_3\}\to\{a_1\exp[ik_1\Delta x],\ a_2\exp[ik_1\Delta x],\ a_3\exp[ik_2\Delta x]\}$ for every Δx. When $k_2=2k_1$ (1:2 resonance case), this transformation becomes $\{a_1,a_2,a_3\}\to\{a_1\exp[i\phi],\ a_2\exp[i\phi],\ a_3\exp[2i\phi]\}$ for every ϕ.

(iii) Mirror reflection $x\to -x$ (left-right symmetry): this is equivalent to the invariance of Eqs. (2) under the transformation $\{a_1,a_2,a_3\}\to\{\overline{a_2},\overline{a_1},\overline{a_3}\}$.

The combination of these fundamental invariance properties requires a number of terms in the Taylor expansions of Eqs. (2) to vanish [6]. As an example, all linear coefficients except diagonal ones must be zero due to requirements (i) and (ii). The invariance (iii) then requires the coefficients of linear terms in the equations for a_1 and a_2 to be complex conjugates of each other (note that these coefficients turn out to be real when deriving amplitude equations systematically), and the linear coefficient in the equation for a_3 to be real. The discussion of nonlinear terms proceeds in the same way, although special attention has to be paid to quadratic terms, for which cases $k_2=2k_1$ and $k_2\neq 2k_1$ are qualitatively different [3]. When the basic wave numbers of the unstable modes are incommensurable, no resonance occurs, and the amplitude equations are free from phase-coupling terms. Among the possible $m:n$ resonance cases, a strong resonance occurs when k_1 and k_2 are in the ratio 1:2, and some quadratic phase-coupling terms now cannot be ruled out by considering the invariance (ii).

After computing the possible cubic terms and limiting Taylor expansions to this order, we arrive at the following system of coupled Ginzburg-Landau equations:

$$\begin{aligned} \dot{a}_1 &= \mu a_1+\delta a_3\overline{a_2}+a_1(\alpha|a_1|^2+\beta|a_2|^2+\gamma|a_3|^2), \\ \dot{a}_2 &= \mu a_2+\overline{\delta a_3}\,\overline{a_1}+a_2(\overline{\alpha}|a_2|^2+\overline{\beta}|a_1|^2+\overline{\gamma}|a_3|^2), \\ \dot{a}_3 &= \mu' a_3+\delta' a_1 a_2+a_3(\alpha'|a_3|^2+\gamma'|a_1|^2+\overline{\gamma'}|a_2|^2), \end{aligned} \tag{3}$$

with $\delta=\delta'=0$ when $k_2\neq 2k_1$. The dot denotes differentiation with respect to t. Note that the mirror symmetry (iii) also requires the coefficients α' and δ' to be real.

An important feature of Eqs. (3) is that they generally do not admit a potential function $\psi(a_i,\overline{a_i})$ such that $\dot{a}_l=-\partial\psi/\partial\overline{a_l}$ for all l (such that $d\psi/dt=-2\Sigma_l|\partial\psi/\partial a_l|^2\leq 0$). Indeed, expressing equalities of cross derivatives of ψ leads to the necessary conditions $\alpha=\overline{\alpha}$, $\beta=\beta$, $\gamma=\overline{\gamma}=\gamma'$, and $\delta=\delta=\delta'$. Interestingly, the analysis of hexagonal convection (e.g., in one-layer Marangoni-Bénard instabilities [11–15]) leads to equations similar to (3) for amplitudes of the three constitutive roll patterns. However, the conditions for existence of a potential are met in this case, such that the dynamics is purely relaxational [13].

Due to the large number of unknown coefficients, a general discussion of the possible solutions and stability properties of Eqs. (3) appears outside the scope of the present work. As in Ref. [8], we thus focus our attention on a particular convective system for which coefficients can be calculated from the governing equations of fluid motion.

II. COMPUTATION OF COEFFICIENTS FOR THE TWO-LAYER MARANGONI-BÉNARD INSTABILITY

In each phase ($i=1,2$), the Boussinesq equations governing the velocity field $\mathbf{V}_i=(U_i,W_i)$ and the deviations of temperature T_i and pressure p_i with respect to the diffusive solution (constant temperature gradient $dT_i/dz=-\beta_i$) are [16]

$$\begin{aligned} \boldsymbol{\nabla}\cdot\mathbf{V}_i &= 0, \\ \kappa_i\Delta T_i+\beta_i W_i &= \dot{T}_i+(\mathbf{V}_i\cdot\boldsymbol{\nabla})T_i, \\ \mu_i\Delta\mathbf{V}_i-\boldsymbol{\nabla}p_i &= \rho_i\{\dot{\mathbf{V}}_i+(\mathbf{V}_i\cdot\boldsymbol{\nabla})\mathbf{V}_i\}, \end{aligned} \tag{4}$$

where ρ_i, μ_i, and κ_i are, respectively, the density, dynamic viscosity, and thermal diffusivity, $\boldsymbol{\nabla}$ and Δ are, respectively, the gradient and the Laplacian operator.

On rigid conducting plates $z=-a_1$ and $z=a_2$ ($a_{i=1,2}$ are the layer thicknesses), the boundary conditions are

$$\mathbf{V}_i=T_i=0, \tag{5}$$

while at the undeformable interface $z=0$ the following conditions hold [10]:

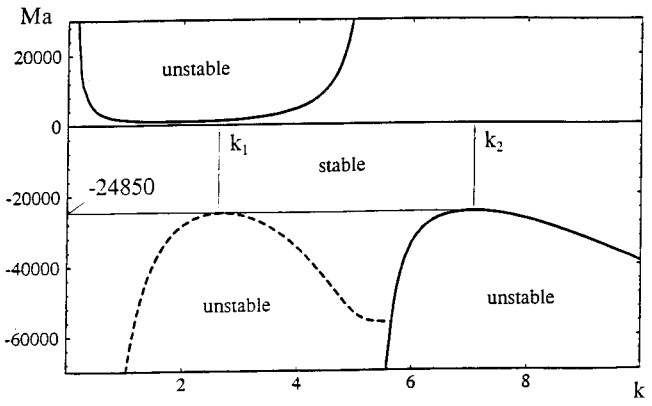

FIG. 1. Linear stability results: Marangoni number Ma as a function of the wave number k for a system with parameters $\rho=\rho_2/\rho_1=0.893$, $\mu=\mu_2/\mu_1=1.02$, $\kappa=\kappa_2/\kappa_1=0.934$, $\lambda=\lambda_2/\lambda_1=0.698$ (methanol-octane) for a value $a=a^*=0.726$ of the thicknesses ratio. Full curves, neutral stability; dashed curves, overstability (the critical frequency is $\omega_c=64.7$).

$$W_1=W_2=0, \quad U_1=U_2, \quad T_1=T_2,$$

$$\lambda_1 \frac{\partial T_1}{\partial z}=\lambda_2 \frac{\partial T_2}{\partial z}, \quad \mu_2 \frac{\partial U_2}{\partial z}-\mu_1 \frac{\partial U_1}{\partial z}=\sigma_T \frac{\partial T_1}{\partial x}, \quad (6)$$

where λ_i is the thermal conductivity and σ_T the interfacial tension variation with temperature.

This problem is put under dimensionless form using a_1 as the length unit, a_1^2/κ_1 as the time unit, and $\Delta T_1=\beta_1 a_1$ as the temperature unit. Then, the linearized stability problem associated with Eqs. (4)–(6) leads to the characteristic relation $\Delta(\sigma,\mathrm{Ma},k,a)=0$ between the growth rate σ of the perturbations, the Marangoni number $\mathrm{Ma}=-\sigma_T \Delta T_1 a_1/\mu_1\kappa_1$, the wave number k, and the ratio of layer thicknesses $a=a_2/a_1$. All other parameters (property ratios) are determined by the choice of liquids: in the following, we use the values $\rho=\rho_2/\rho_1=0.893$, $\mu=\mu_2/\mu_1=1.02$, $\kappa=\kappa_2/\kappa_1=0.934$, and $\lambda=\lambda_2/\lambda_1=0.698$, representative of the methanol (layer 1)–n-octane (layer 2) configuration. The numerically computed stability diagram for these parameters values is represented in Fig. 1.

Figure 1 is obtained for the particular value $a=a^*=0.726$ of the thicknesses ratio, for which an asymptote exists in the neutral stability ($\sigma=0$) limit at $k\simeq 5.4$, separating regions where the monotonic instability sets in either at low wave numbers by heating from the methanol side ($\mathrm{Ma}>0$), or at high wave numbers by heating from the octane side ($\mathrm{Ma}<0$). This behavior is connected with the fact that thermal diffusion times are similar for both liquid layers [17]. Furthermore, it is seen that an overstable ($\sigma=i\omega$) branch exists when $\mathrm{Ma}<0$, and that its threshold coincides with the threshold of the monotonic mode at the critical Marangoni number $\mathrm{Ma}_c=-24\,850$. This situation is occasional ($a=a^*$), and for increasing octane thickness $a>a^*$, the monotonic mode is first critical, while the oscillating mode becomes more dangerous when $a<a^*$. The point (Ma_c,a^*) thus defines a codimension-2 point for this problem [13]. In order to investigate the behavior in the vicinity of this CTP, we use the real parameters μ and μ', defined by Eqs. (3) and representing the real part of the growth constants of both modes. Thus, μ and μ' vanish at the CTP, and can be linearly approximated in its vicinity:

$$\mu=s_1(\mathrm{Ma}-\mathrm{Ma}_c)+s_2(a-a^*),$$

$$\mu'=s_1'(\mathrm{Ma}-\mathrm{Ma}_c)+s_2'(a-a^*). \quad (7)$$

It is not the purpose of this paper to describe the particular technique used to compute nonlinear coefficients of the amplitude equations (3). We just mention that our method is a mode projection technique (which is equivalent to standard perturbation techniques), similar to those presented in Refs. [14,15] although for different problems. As expected, all these systematic methods also lead to Eqs. (3). The accuracy of numerical computations of the coefficients was successfully tested in the two-layer problem with the different technique used in Ref. [18] and in the one-layer problem with the value of the hysteresis of hexagons reported in Ref. [19] in the finite-depth case. The values obtained in the present work are presented in Table I, for both cases of nonresonant and resonant interactions.

III. RESULTS AND DISCUSSIONS

A. Nonresonant case

Substituting $a_l=r_l \exp[i\varphi_l]$ in the system (3) with $\delta=\delta'=0$ leads to equations for the amplitudes r_l that are decoupled from those governing the phases φ_l. The only possible solutions with stationary amplitudes are

TABLE I. Coefficients of the amplitude equations for nonresonant ($k_1=2.67$, $k_2=7.03\neq 2k_1$) and resonant ($k_1=3$, $k_2=6=2k_1$) cases. The system parameters are $\rho=\rho_2/\rho_1=0.893$, $\mu=\mu_2/\mu_1=1.02$, $\kappa=\kappa_2/\kappa_1=0.934$, $\lambda=\lambda_2/\lambda_1=0.698$ (methanol-octane), and the CTP thickness ratio a^* and critical Marangoni number Ma_c are given for both cases.

	Nonresonant	Resonant		Nonresonant	Resonant
a^*	0.726	0.749	δ	0	$-14.7-18.4i$
Ma_c	$-24\,850$	$-26\,895$	δ'	0	0.643
ω_c	64.7	62.1	α	$-0.199-0.126i$	$-0.262-0.193i$
s_1	-7.07×10^{-4}	-6.9×10^{-4}	β	$0.270-0.393i$	$0.234-0.447i$
s_2	-34.3	-46.8	γ	$27.5+18.2i$	$-3.46+0.373i$
s_1'	-1.48×10^{-3}	-1.28×10^{-3}	α'	-14.6	-13.8
s_2'	111	278	γ'	$-0.997+3.74i$	$-0.235+1.34i$

$$r_1=r_2=r_3=0 \quad \text{[diffusive rest state } (O)\text{]}, \tag{8}$$

$$r_1=r_2=0, \quad r_3^2=-\mu'/\alpha' \quad \text{[steady convection (SC)]}, \tag{9}$$

$$r_3=r_{2(1)}=0, \quad r_{1(2)}^2=-\mu/\alpha_R,$$

$$\text{[traveling waves (TW)]}, \tag{10}$$

$$r_3=0, \quad r_1^2=r_2^2=-\mu/(\alpha_R+\beta_R)$$

$$\text{[standing waves (SW)]}, \tag{11}$$

$$r_{1(2)}=0, \quad r_{2(1)}^2=(\mu'\gamma_R-\mu\alpha')/(\alpha_R\alpha'-\gamma_R\gamma_R'),$$
$$r_3^2=(\mu\gamma_R'-\mu'\alpha_R)/(\alpha_R\alpha'-\gamma_R\gamma_R')$$

$$\text{[mixed solution SC+TW } (M_2)\text{]}, \tag{12}$$

$$r_1^2=r_2^2=(\mu'\gamma_R-\mu\alpha')/[\alpha'(\alpha_R+\beta_R)-2\gamma_R\gamma_R'],$$
$$r_3^2=[2\mu\gamma_R'-\mu'(\alpha_R+\beta_R)]/[\alpha'(\alpha_R+\beta_R)-2\gamma_R\gamma_R']$$

$$\text{[mixed solution SC+SW } (M_3)\text{]}, \tag{13}$$

where an index R means the real part of a coefficient. Existence conditions for each kind of solution are directly obtained from Eqs. (9)–(13), by requiring the positiveness of squared amplitudes r_I^2. This leads to existence domains limited by lines going through the origin in the (μ,μ') unfolding plane (see Fig. 2). Stability conditions may also be obtained analytically, although for conciseness results are not reproduced here. Figure 2 summarizes the relevant results, i.e., the map of possible behaviors in the (μ,μ') plane. The corresponding bifurcation diagrams are represented in Fig. 3. For each solution, nonlinear corrections to the linear frequencies are computed from the imaginary part of the amplitude equations (an index I means imaginary part):

$$\dot\varphi_1=\omega_1=\alpha_I r_1^2+\beta_I r_2^2+\gamma_I r_3^2,$$

$$\dot\varphi_2=\omega_2=-\alpha_I r_2^2-\beta_I r_1^2-\gamma_I r_3^2,$$

$$\dot\varphi_3=\omega_3=\gamma_I'(r_1^2-r_2^2), \tag{14}$$

where $\omega_{i=1,2,3}$ are constant [and can be computed from Eqs. (8)–(13) for each solution], such that $\varphi_i=\omega_i t+\varphi_{i0}$, and φ_{i0} is arbitrary.

Now, for symmetric solutions ($r_1=r_2$), Eqs. (14) lead to $\omega_2=-\omega_1$ and $\omega_3=0$: according to Eq. (1), the perturbation fields are thus periodic with a single frequency $\omega=\omega_c+(\alpha_I+\beta_I)r_1^2+\gamma_I r_3^2$. This is the case for both SW and M_3 solutions. The SC solution also falls into this category, but the amplitudes of waves are zero, such that this solution is effectively steady. It is also checked that the TW solution is time periodic, while the M_2 solution (dissymmetric) is the superposition of two traveling waves with incommensurate phase velocities $v=\omega/k_1=(\omega_c+\alpha_I r_1^2+\gamma_I r_3^2)/k_1$ and $v'=\omega'/k_2=\gamma_I' r_I^2/k_2 \ll v$ (note that the direction of propagation is the same because $\gamma_I'>0$, as seen in Table I). This M_2 solution is thus quasiperiodic both in time and in space (because the constitutive wave numbers k_1 and k_2 are also incommensurate). However, the stability results indicate that it is always unstable for the present parameter values.

In Fig. 2, it is seen that in a large part of the diagram, no stable steady solution exists. In particular, as also seen in Fig. 3, the Hopf bifurcation occurring at $\mu=0$ (for $a<a^*$, i.e., $\mu'<0$) results in supercritical TW and subcritical SW, which are both unstable [6]. Since no saturation is obtained from cubic terms in this case (this is due to the fact that $\alpha_R+\beta_R>0$), higher-order (quintic) terms should be included in amplitude equations. Such a procedure might result in standing waves of finite amplitude existing in a certain subcritical region. Stable solutions exist when $a>a^*$, under the form of a SC supercritical solution (bifurcating from the rest state on the axis $\mu'=0$, $\mu<0$), undergoing a secondary bifurcation to the mixed solution M_3 when the constraint is increased (at $\mu'/\mu=\alpha'/\gamma_R=-0.531$). An interesting feature

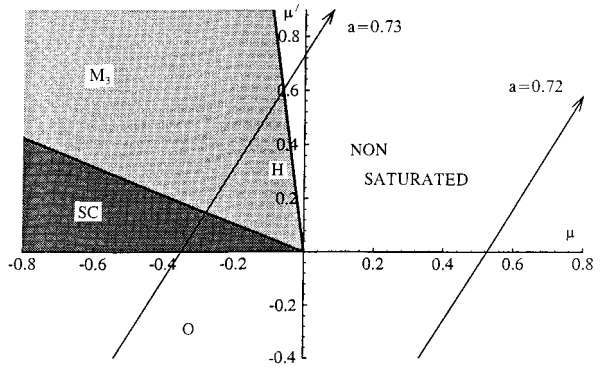

FIG. 2. Stability map in the nonresonant case, as a function of the linear growth constants μ (of the waves) and μ' (of steady convection). Arrows indicate paths followed when the Marangoni number is increased, for two values of the thickness ratio a. Only stable solutions are indicated: O=reference state, SC=steady convection, M_3=mixed (spatially quasiperiodic) mode. Nonsaturated growth occurs for $\mu>0$, and at the right of the Hopf bifurcation line H.

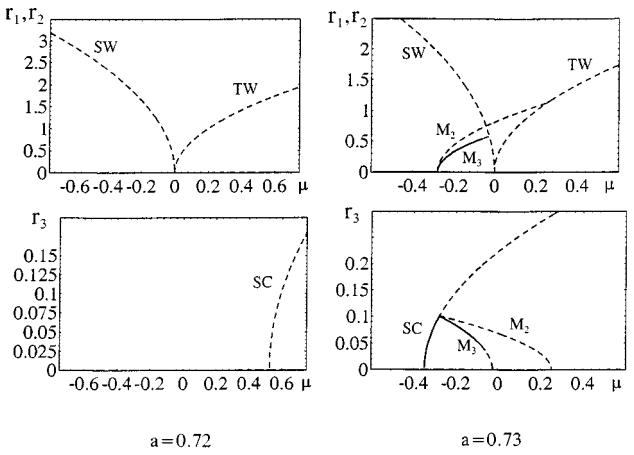

FIG. 3. Bifurcation diagrams for the qualitatively different cases $a=0.72<a^*$ (left) and $a=0.73>a^*$ (right). The amplitudes of the waves $r_{1,2}$ and of steady convection r_3 are represented as a function of the growth constant μ of waves, for a displacement along the arrows labeled $a=0.72$ and $a=0.73$ of Fig. 2. Full curves represent stable states, while dashed curves represent unstable states. SC =steady mode, TW (SW)=traveling (standing) waves, M_2=SC+TW, M_3=SC+SW.

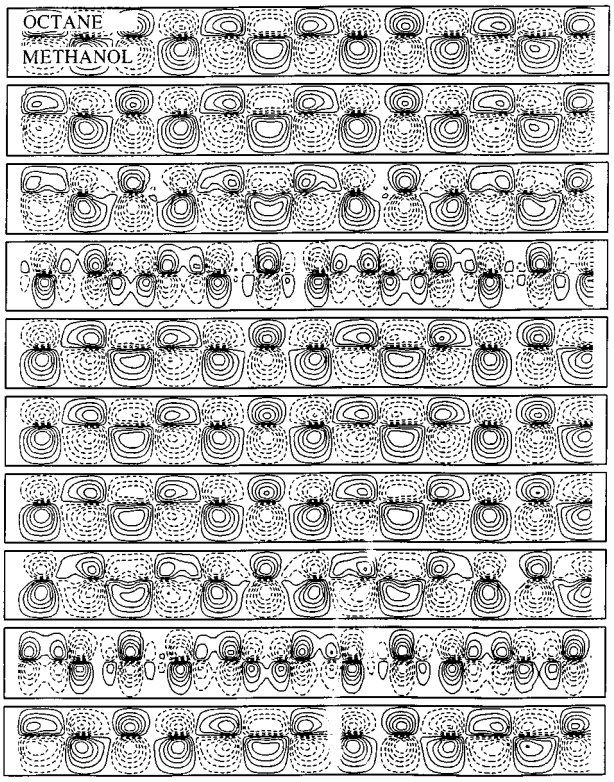

FIG. 4. Representation of the stable mixed M_3 solution ($a=0.73$, $\mathrm{Ma}=-24760$): stream function in both layers. The system is quasiperiodic along the layers (wave numbers $k_1=2.67$ and $k_2=7.03$), and oscillates in time with the pulsation $\omega\simeq\omega_c=64.7$. The stream function is rescaled at each snapshot ($\Delta t=T/10\simeq 9.7\ 10^{-3}$). Time runs downwards.

of this solution is its spatial quasiperiodicity (the constitutive modes have incommensurate wave numbers k_1 and k_2). However, contrary to the M_2 solution, it has only one temporal frequency ω (which can be shown to be decreasing with increasing Marangoni number). This M_3 solution, represented in Fig. 4, finally undergoes a third (Hopf) bifurcation when the constraint is increased, slightly before merging with the unstable subcritical SW branch at the point where the amplitude of the steady component r_3 vanishes [at $\mu'/\mu=2\gamma_R'/(\alpha_R+\beta_R)=-28.1$]. As Figs. 2 and 3 show, no stable saturated solution exists beyond the line H of the Hopf bifurcation, thus again requiring calculation of higher-order contributions.

B. Resonant case

For values of fluid properties selected in Sec. II, the condition $k_2=2k_1$ is clearly not satisfied (see Fig. 1). Rather than changing fluid properties in order to achieve exact resonance at threshold (this is possible, e.g., by increasing the viscosity ratios ν_2/ν_1 and μ_2/μ_1, and adjusting the thickness ratio $a=a_2/a_1$), we preferred to force resonance by arbitrarily selecting basic wave numbers, say $k_1=3$ and $k_2=6$ (thus requiring the system to be periodic in the x direction with the period $\Delta x=\pi/3$). In order for the thresholds of oscillatory and stationary modes to coincide, we have to adjust the value of a, such that the CTP now occurs for ($\mathrm{Ma}_c=-26\,895$, $a^*=0.7488$). Note that this somewhat artificial procedure might lead to some qualitative accordance with behaviors observed in a realistic system when the constraint is large enough, such that large bands of wave numbers, including k_1 and k_2, are unstable [this could be checked by direct numerical simulation of Eq. (4)–(6)]. Moreover, some of the conclusions made in this section are quite general, as they are based on a discussion of the quadratic system, for which suitable rescalings eliminate most of the coefficients. Thus, in order to exploit some of the predictions made here for other resonant systems, only the quadratic coefficients δ and δ' need to be computed (which is much easier than the computation of cubic coefficients). The new set of coefficients for full amplitude Eqs. (3) is presented in Table I.

1. Quadratic system

We first concentrate on the role of quadratic nonlinearities. In this respect, it should be stressed that, due to their perturbative origin, the strict validity of Eqs. (3) may only be guaranteed in some neighborhood of the origin $a_1=a_2=a_3=0$. Since $\delta=|\delta|\exp[i\varphi_\delta]$ and δ' are finite quantities, the dynamics near this point should be governed by the quadratic system obtained by neglecting cubic nonlinearities in Eqs. (3). This becomes clearer by introducing the change of scales

$$t\to\mu^{-1}t,$$

$$(a_1,a_2)\to\left|\frac{\mu\mu'}{|\delta|\delta'}\right|^{1/2}(a_1,a_2),$$

$$a_3\to\frac{\mu}{|\delta|}a_3, \tag{15}$$

which allows us to rewrite the system (3) as

$$\begin{aligned}
\dot a_1&=a_1+\exp[i\varphi_\delta]a_3\overline{a_2}+a_1(\tilde\alpha|a_1|^2+\tilde\beta|a_2|^2+\tilde\gamma|a_3|^2),\\
\dot a_2&=a_2+\exp[-i\varphi_\delta]a_3\overline{a_1}+a_2(\tilde{\bar\alpha}|a_2|^2+\tilde{\bar\beta}|a_1|^2+\tilde{\bar\gamma}|a_3|^2),\\
\dot a_3&=\chi(a_3+sa_1a_2)+a_3(\tilde\alpha'|a_3|^2+\tilde\gamma'|a_1|^2+\tilde{\bar\gamma}'|a_2|^2),
\end{aligned} \tag{16}$$

where φ_δ is the phase of the quadratic coefficient δ, $\chi=\mu'/\mu$, $s=\mathrm{sgn}(\chi/\delta')$, and the cubic coefficients with tilde are defined by

$$\tilde\alpha=s\frac{\alpha\mu'}{\delta'|\delta|},\quad \tilde\beta=s\frac{\beta\mu'}{\delta'|\delta|},\quad \tilde\gamma=\frac{\gamma\mu}{|\delta|^2},$$

$$\tilde\alpha'=\frac{\alpha'\mu}{|\delta|^2},\quad \tilde\gamma'=s\frac{\gamma'\mu'}{\delta'|\delta|}. \tag{17}$$

These coefficients are proportional to μ or μ'. Near the CTP ($\mu,\mu'\ll 1$), it should thus be possible to neglect corresponding terms, provided that the amplitudes a_1, a_2, and a_3 stay bounded (i.e, of order unity). Most of this section is devoted to a discussion of the regions of the (μ,μ') plane where this condition is satisfied. In fact, cubic terms are essential in some limiting cases, as will be seen later. For the moment, neglecting them and separating amplitudes and phases in the

usual manner $a_l = r_l \exp[i\varphi_l]$, we arrive at the four-dimensional dynamical system

$$\dot{r}_1 = r_1 + r_2 r_3 \cos(\varphi_\delta - \varphi),$$

$$\dot{r}_2 = r_2 + r_1 r_3 \cos(\varphi_\delta + \varphi),$$

$$\dot{r}_3 = \chi(r_3 + s r_1 r_2 \cos\varphi),$$

$$\dot{\varphi} = \frac{r_2 r_3}{r_1} \sin(\varphi_\delta - \varphi) - \frac{r_1 r_3}{r_2} \sin(\varphi_\delta + \varphi) - \chi s \frac{r_1 r_2}{r_3} \sin\varphi, \tag{18}$$

where $\varphi = \varphi_1 + \varphi_2 - \varphi_3$ is the only quantity involving phases coupled to the amplitudes r_i. The only steady nontrivial solutions of the system (18) are found to be the following:
The symmetric solution (SS):

$$r_1^2 = r_2^2 = (s\ \cos\varphi_\delta)^{-1},$$

$$r_3^2 = (\cos\varphi_\delta)^{-2}, \quad \varphi = n\pi \quad (n = 0,1), \tag{19}$$

which exists provided $s\cos\varphi_\delta > 0$.
The asymmetric solutions (AS):

$$r_1^2 = \frac{(1+q^2)(1+2\chi^{-1})}{s\ \cos\varphi_\delta\ q^2\{1 \mp [1+2\chi^{-1}(1+q^2)]^{1/2}\}},$$

$$r_2^2 = \frac{(1+q^2)(1+2\chi^{-1})}{s\ \cos\varphi_\delta\ q^2\{1 \pm [1+2\chi^{-1}(1+q^2)]^{1/2}\}},$$

$$r_3^2 = -\frac{(2+\chi)(1+q^2)}{2q^2},$$

$$\tan\varphi = \pm\frac{1}{q}[1+2\chi^{-1}(1+q^2)]^{1/2}, \tag{20}$$

where $q = \tan\varphi_\delta$. The AS exist, provided $s\cos\varphi_\delta > 0$ and $\chi < -2(1+q^2)$. Contrary to the SS, the AS do not individually obey the left-right symmetry (iii). However, they are mapped onto each other by applying the corresponding transformation.

A general discussion of the properties of the system (18) will not be attempted here. In the following, we restrict our analysis to cases where $\delta' > 0$ and $\cos\varphi_\delta < 0$ (see Table I). Still, this will allow comparison with some results of Fujimura and Renardy [8] (denoted FR in what follows), as these conditions are also fulfilled in their analysis. Thus, $s\cos\varphi_\delta > 0$ if $s = -1$, i.e., $\chi = \mu'/\mu < 0$ is a necessary condition for the SS and the AS to exist. Moreover, the AS can only exist provided $\chi < -2(1+q^2)$. The stability conditions may be obtained analytically for the SS: computing eigenvalues of the Jacobian matrix leads to

$$\lambda_{1,2}^{SS} = \frac{\chi \pm \sqrt{\chi(\chi+8)}}{2} \tag{21}$$

whose real parts are always negative for $\chi = \mu'/\mu < 0$ (i.e., in the existence region of the SS), and thus correspond to stable directions when $\mu > 0$ and to unstable directions when $\mu < 0$ [because the eigenvalues have to be multiplied by μ in virtue of the scalings (15)]. The other two eigenvalues are

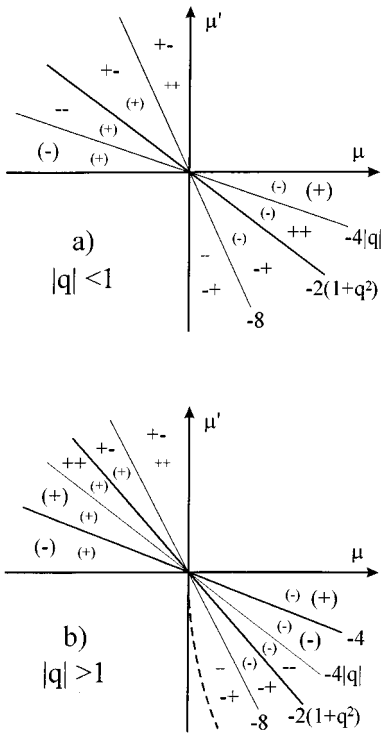

FIG. 5. Stability diagram of the symmetric solution (SS) of the quadratic system for cases $|q| < 1$ (a) and $|q| > 1$ (b), and for $\delta' > 0$ and $\cos\varphi_\delta < 0$. On the axes, μ and μ' denote, respectively, the linear growth constants of waves and of steady convection. In each sector (delimited by lines of indicated slope $\chi = \mu'/\mu$), the signs of the real part of the four eigenvalues are given. A pair of complex conjugate eigenvalues is denoted by $(+)$ if unstable and by $(-)$ if stable. Larger symbols correspond to eigenvalues (22), smaller ones to eigenvalues (21). The dashed curve in case (b) is the parabola $\mu'^2/\mu = q^2\delta'\,\delta_R/\alpha_R$ [Eq. (24)].

$$\lambda_{+,-}^{SS} = \frac{\chi + 4 \pm \sqrt{\chi^2 - 16q^2}}{2}, \tag{22}$$

the discussion of which depends on whether $|q| > 1$ or $|q| < 1$, and is summarized in Fig. 5.

Note that $q = 1.25$ here and $q = -5.36$ in FR such that $|q| > 1$ in both cases, and we are in the situation sketched in Fig. 5(b). We now concentrate on the case $\mu > 0$ (and $\mu' < 0$), i.e., the only quadrant where SS may be stable. According to Eq. (22), when $|q| > 1$, the SS solution is stable in the range $-4 > \chi > -2(1+q^2)$ ($= -5.13$ here, and -59.4 in FR). This defines a sector of stability in Fig. 5(b). At $\chi = -4$, the SS solution undergoes a Hopf bifurcation, leading to time-dependent behaviors that diverge in the dynamics described by the quadratic system (18). Including cubic terms leads to 3-torus solutions (as discussed by FR). However, these behaviors are not investigated here, as they are not fully governed by the quadratic system. At the other end of the stability interval, i.e., at $\chi = -2(1+q^2)$, the SS solution undergoes a bifurcation to an AS solution (which starts to exist there and is stable in some range provided $|q| > 1$).

When $|\chi|$ is increased (χ is decreased), the stable AS may lose stability itself, or keep stable up to $\chi \to -\infty$. This again depends on the value of q. A numerical computation of the eigenvalues characterizing the stability of the AS shows that

it stays stable for every $\chi<-2(1+q^2)$, provided $|q|>2.297$, while it becomes unstable at a certain χ^* for $|q|<2.297$. Thus, the FR results differ from ours at this stage, because the AS stay stable in their analysis (except for very large $|\chi|$ where the quadratic system is not valid, and cubic terms destabilize the AS, leading to noise-sustained oscillations [8]). Here, the AS undergoes a Hopf bifurcation at $\chi^*=-5.65$. No stable fixed point of the quadratic system (18) exists beyond that point, such that time-dependent motions occur that first take the form of limit cycles centered around both unstable AS foci [see Fig. 6(a)]. Note that these cycles are mirror images of each other with respect to the left-right symmetry (symbolized by the dot-dashed line in Fig. 6).

The scenario of transition to chaos that we describe now [obtained by numerical integration of the QUADRATIC system (18) with a fourth-order Runge-Kutta procedure with relative accuracy 10^{-10}] has already been encountered in Lorenz-like models of convection [20], and was first postulated by Arneodo *et al.* [21]. For larger $|\chi|$, both cycles of Fig. 6(a) grow symmetrically and approach the unstable SS (saddle point). At a certain χ (say χ_0^H), the periodic trajectories tend to homoclinic orbits (saddle connections) of the SS, approaching it infinitely close along one of its stable directions (the least stable), and leaving it along the unstable direction. At this point [see Fig. 6(b)], the period of each cycle is infinite, and the two cycles merge into a new ''double-loop'' cycle (hereafter denoted C-2), via a mechanism thought to be a homoclinic gluing [22] bifurcation. Increasing $|\chi|$ again, leads to a deformation of the symmetric C-2 cycle [see Fig. 6(c)], followed by a symmetry-breaking (SB) bifurcation (say, at $\chi=\chi_1^{\mathrm{SB}}$), leaving the symmetric C-2 cycle unstable to two stable dissymmetric C-2 cycles [see Fig. 6(d)]. Increasing $|\chi|$ again leads to a new homoclinization of these stable cycles at the SS saddle point. At this moment [at $\chi=\chi_1^H$, see Fig. 6(e)], both C-2 cycles become glued into a C-4 cycle (four loops). The resulting cycle is symmetric in a first stage [Fig. 6(f)], but undergoes a symmetry-breaking bifurcation at χ_2^{SB}. At χ_2^H [Fig. 6(g)], both C-4 cycles become glued into a C-8 cycle, and the process repeats, the values χ_n^{SB} (at which the C-2^n cycle becomes dissymmetric) and χ_n^H (at which the two C-2^n cycles merge) converging geometrically to a value estimated at $\chi_\infty=-135$, which corresponds to the onset of chaos [the convergence rate is estimated at $(\chi_{n+1}^H-\chi_n^H)/(\chi_n^H-\chi_{n-1}^H)\rightarrow 2.6$]. Fig. 6(h) exhibits a magnification of a chaotic trajectory ($\chi=-150<\chi_\infty$) near the SS saddle point. Note that this route to chaos actually differs from the more classical period-doubling sequence in many respects [20–24] (divergence of the period of orbits at bifurcation points χ_n^H, dependence of the geometrical convergence rate on the saddle index leading to ratios different from the Feigenbaum ratio, and the importance of symmetry and symmetry-breaking effects).

The behaviors just described have been obtained from the quadratic system (18), and are thus strictly valid near the CTP, i.e., in the limit $\mu,\ \mu'\rightarrow 0,\ \chi=O(1)$ [this has been checked from a simulation of the full cubic system (16)]. The result is that a transition to chaos occurs when $|\chi|$ is increased. It would thus be tempting to conclude that at the threshold of instability of the motionless state ($\mu=0,\quad \mu'<0$), the system undergoes a direct transition to chaos. We now show that this surprising behavior is a consequence of the truncation to the quadratic system (16), which may be resolved by reintroducing cubic terms. Thus, the following developments aim to determine what is the scenario of bifurcations leading from the motionless state to the above-described chaotic behaviors, when *increasing* the driving constraint, i.e., following arrows such as those represented in Fig. 2. It would be rather unusual that chaos occurs at the first bifurcation point, i.e., at $\mu=0$, $\mu'=O(1)<0$. In this limit ($\chi\rightarrow-\infty$), the quadratic system (18) is no longer valid. To show this, note that one of the components of the AS (20) diverges [$r_{1(2)}\sim(-\chi)^{1/2}$] for $\chi\rightarrow-\infty$. Using (15) to return to original variables, one obtains that the corresponding physical solution is finite [in fact, proportional to $\mu'=O(1)$] for $\mu\rightarrow 0$. Thus, cubic terms need to be reintroduced in this limit, and we must return to Eqs. (16).

2. Cubic system

The full system (16) admits ''pure solutions'' (among others [8]), such as the TW solution

$$a_3=a_2=0,\quad |a_1|^2=r_1^2=-\tilde{\alpha}_R^{-1}\sim(\mu')^{-1}, \tag{23}$$

which is identical to Eq. (10). Note that the phase of a_1 varies linearly with time as $\dot{\varphi}_1=\tilde{\alpha}_I r_1^2=-\tilde{\alpha}_I/\tilde{\alpha}_R=-\alpha_I/\alpha_R$ (nonlinear frequency shift). As (23) bifurcates from the trivial state at $\mu=0$, there must be a region near the $\mu=0$, $\mu'=O(1)<0$ axis where cubic terms are essential (and where the TW solution has lower amplitude than the AS). On the contrary, the quadratic system has been shown to determine the dynamics when $\chi=O(1)$ and $\mu,\mu'\rightarrow 0$ (in which case the AS is smaller than the TW solution). Thus, the limit of validity of the quadratic system should occur in a region where amplitudes of TW and AS are comparable. Using Eqs. (20) and (23), it is found that equality between amplitudes of AS and TW occurs for $\chi/q^2\cos\varphi_\delta=\tilde{\alpha}_R^{-1}$ (in the limit $\mu,\mu'\rightarrow 0$), which gives

$$\frac{\mu'^2}{\mu}=\frac{q^2\delta'\delta_R}{\alpha_R}, \tag{24}$$

i.e., a parabola $\mu=0.0177\mu'^2$ in the (μ,μ') plane [dashed curve in Fig. 5(b)].

We now discuss the stability characteristics of TW. For this solution, analytical computations of eigenvalues are possible [8] by perturbing the system (16) according to $a_1=(r_1+b_1)\exp[-i\alpha_I t/\alpha_R]$, $a_2=b_2$, $a_3=b_3\exp[-i\alpha_I t/\alpha_R]$, and linearizing with respect to b_i's. We first get $\dot{b}_1=-(1+i\alpha_I/\alpha_R)(b_1+\bar{b}_1)$, decoupled from equations governing b_2 and b_3, and leading to eigenvalues -2 (stable) and 0 (motion along the limit cycle). The equations for b_2 and b_3 lead to two other eigenvalues λ (governing stability), which satisfy

$$\left(\lambda-1+\frac{\overline{\beta}}{\alpha_R}\right)\left(\lambda-\chi+\frac{\gamma'}{\alpha_R}-i\,\frac{\alpha_I}{\alpha_R}\right)+\frac{\chi\overline{\delta\delta'}}{\alpha_R\mu'}=0. \tag{25}$$

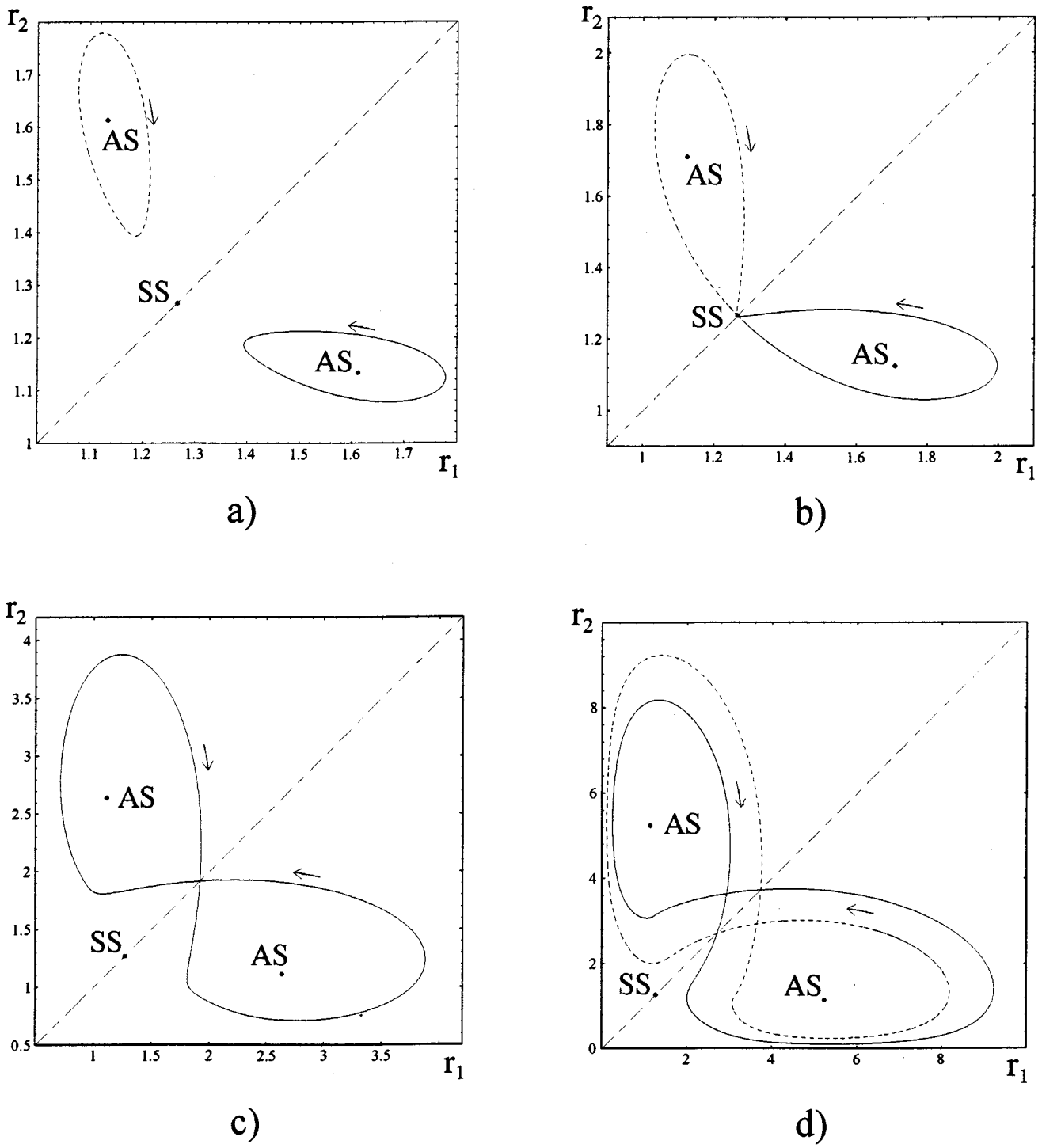

FIG. 6. Time-dependent behaviors of the four-dimensional quadratic system occurring for $\chi<\chi^*=-5.65$, projected in the (r_1,r_2) plane. The left-right symmetry is represented as a dot-dashed line. Only stable cycles are represented. Fixed points (unstable) are the saddle point SS (symmetric mode), and the saddle-foci AS (asymmetric modes). (a) limit cycles (mirror images with respect to the left-right symmetry) for $\chi^*>\chi>\chi_0^H$. (b) Saddle connections (homoclinic orbits) of the SS saddle point at $\chi=\chi_0^H=-6.09$. (c) Symmetric double-loop cycle (C-2) for $\chi_0^H>\chi>\chi_1^{SB}$. (d) Two stable dissymetric C-2 cycles (mirror images) for $\chi_1^{SB}>\chi>\chi_1^H$. (e) Homoclines of the saddle point SS at $\chi=\chi_1^H=-45.0$. (f) Symmetric C-4 cycle for $\chi_1^H>\chi>\chi_2^{SB}$. (g) Two dissymmetric C-4 cycles at the point $\chi=\chi_2^H=-101.5$ of homoclinic bifurcation. (h) Trajectories in the vicinity of the saddle point in the chaotic regime ($\chi=-150$).

Two different limiting cases of this equation are studied. The first one is $\mu\to 0$, $\mu'=O(1)<0$, i.e., near the bifurcation point from the motionless state ($\chi\to-\infty$). It is found that eigenvalues tend to $\lambda_1=\chi<0$ (stable) and $\lambda_2=1-\beta/\alpha_R+\delta\delta'/\alpha_R\mu'$. These eigenvalues reflect the fact that for $\chi\to-\infty$ the a_3 amplitude is adiabatically slaved [25] to a_1 and a_2. Indeed, in the third of Eqs. (16), $a_3\to a_1a_2$ when $s=-1$ and $\chi\to-\infty$. Substituting this expression in the first two Eqs. (16), and neglecting $|a_3|^2$ (fourth order), we get a standard TW-SW competition [6] with cubic interaction co-

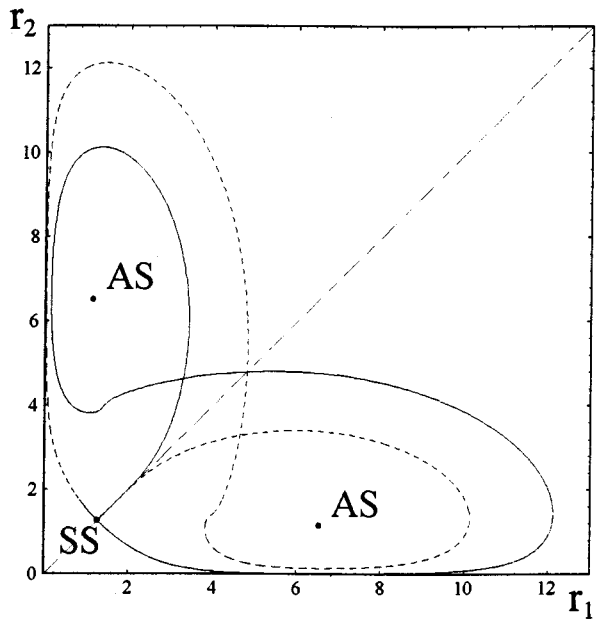

e)

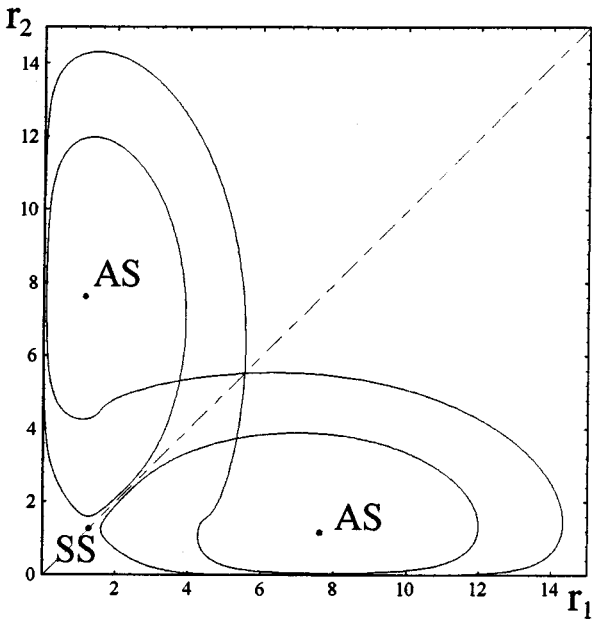

f)

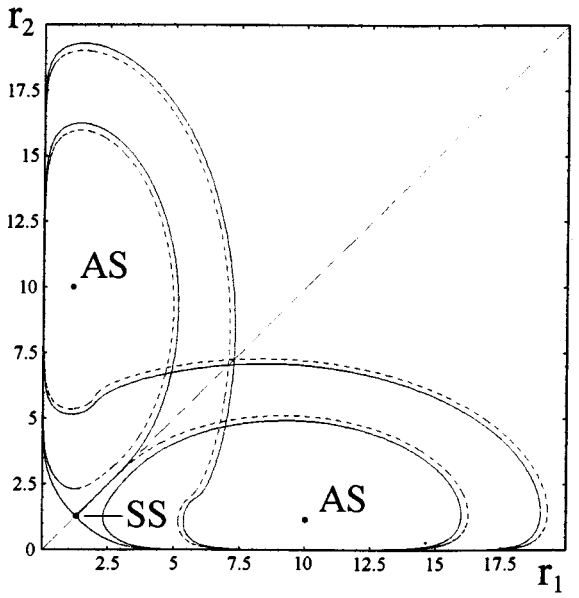

g)

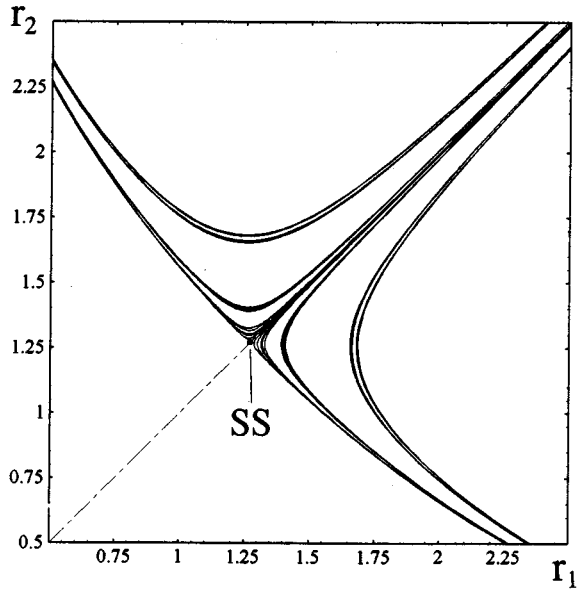

h)

FIG. 6 (*Continued*).

efficient $\widetilde{\beta}+\exp[i\varphi_\delta]$ and self-interaction coefficient $\widetilde{\alpha}$. Therefore, as $\widetilde{\alpha}_R<0$ here, the supercritical TW solution is stable against SW if $\widetilde{\alpha}_R-\widetilde{\beta}_R-\cos\varphi_\delta>0$ (equivalently $\lambda_{2R}<0$), and unstable in the opposite case. Thus, the TW is stable at the bifurcation point of waves if $0>\mu'>\delta_R\delta'/(\beta_R-\alpha_R)=-19.1$. As we study the vicinity of the CTP, we assume in the following that this condition is satisfied.

The second limiting case is $\chi=O(1)$, and $\mu,\mu'\to 0$ [where the quadratic system (18) is valid, and possesses attracting solutions depicted in Fig. 6]. Equation (25) shows that $\lambda_{1,2}=\pm(\chi\delta\delta'/\alpha_R\mu')^{1/2}$, and one of these eigenvalues has a positive real part. TW solutions have thus lost stability in between the two different regions of the (μ,μ') plane that we have investigated. The threshold may be found by substituting $\lambda=i\Omega$ in (25), which in fact exactly leads to the condi-

tion (24) for $\mu,\mu' \to 0$. Thus, on the parabola $\mu = 0.0177\mu'^2$ [see Fig. 5(b)], the TW can be supposed to undergo a bifurcation to an AS, which is indeed confirmed by direct numerical integration of Eqs. (16).

CONCLUDING RESULTS AND SUMMARY

We now summarize the developments made in this section for the quadrant $\mu > 0$, $\mu' < 0$, and supplement them with numerical results obtained from the full cubic system (16). The first bifurcation from the motionless state occurs at $\mu = 0$ to a pure stable TW solution (of the cubic system), which undergoes a secondary bifurcation to an AS at $\mu = 0.0177\mu'^2$ [dashed line of Fig. 5(b)]. For values of $\mu > 0.0177\mu'^2$ (e.g., increasing the Marangoni number Ma), the bifurcated AS is first stable, then undergoes a tertiary Hopf bifurcation, leading to a situation similar to Fig. 6(a) (note that the unstable TW solution is not represented in this figure, and would in fact lie much further from the origin than the represented SS and AS). For increasing values of μ, a transition to chaos occurs via an infinite sequence of bifurcations qualitatively similar to that described in Fig. 6 (which corresponds to decreasing values of μ). However, contrary to this latter sequence, the transitions observed here when increasing μ cannot be described by quadratic nonlinearities alone, and should thus be considered with some precaution, in view of the remarks made above. Thus, the sequence observed when increasing Ma should accumulate on a curve in the (μ,μ') plane, which might be of some parabolic form $\mu \sim \mu'^2$ (although this has not been checked). Beyond this line, the system is in a chaotic state similar to Fig. 6(h). Now, when increasing Ma again, a *reverse* transition represented in Fig. 6 occurs [Figs. 6(h)–6(a)], the remaining two limit cycles of Fig. 6(a) finally collapsing on the AS (at $\chi = \chi^* = -5.65$). As shown above, the AS stay stable for a short range [up to $\chi = -2(1+q^2) = -5.13$], and both AS states in turn collapse on the SS, which becomes the only (stable) steady solution at this point. It was also seen that at $\chi = -4$, this SS state undergoes a Hopf bifurcation to a quasiperiodic state (3-torus) not investigated further in this work.

Finally, we briefly describe some results obtained via numerical integration of the full set of equations (16) in other quadrants, illustrating the wide variety of behaviors possible for this resonant system. We insist on the qualitative validity of these results, due to the $O(1)$ magnitude of the quadratic coefficients (see also [26]). In the quadrant $\mu < 0$, $\mu' > 0$ (where no stable fixed point exists), the (r_1, r_2, r_3, φ) phase-space trajectory eventually describes a limit cycle (with frequency $\omega' \ll \omega_c$), thus again leading to temporal quasiperiodicity of the physical variables (3-torus). The small value of the frequency ω' is due to the fact that the system spends the largest part of the oscillation period near the $r_1 = 0$, $r_2 = 0$ coordinate line (where the system is in a quasi-steady state), and undergoes quick deviations (similar to relaxation oscillations) at moments that may eventually become irregularly spaced in time. During these high-frequency (ω_c) relaxation periods, the amplitude of the steady mode changes sign (the phase undergoes a jump of π), such that the system may be viewed as regularly switching between two quasi-steady states with reversed convective velocities. When destabilizing the system with respect to the oscillating mode (quadrant $\mu > 0$, $\mu' > 0$), intricate phase-space trajectories reveal that complicated deterministic chaos occurs whose structure has not been investigated further.

ACKNOWLEDGMENTS

We thank A. Rednikov, M. G. Velarde, A. A. Nepomnyashchy, G. Dewel, P. Borckmans, A. Dewit, and J. Halloy for stimulating discussions. We are especially grateful to M. A. Zaks, from the Universität Postdam, for judicious advice concerning transitions to chaos. P.C. acknowledges financial support from the EC network ERBCHRXCT930106 for his stay at Universidad Complutense de Madrid. This text presents research results of the Belgian Programme on InterUniversity Poles of Attraction (PAI 21) initiated by the Belgian State, Prime Minister's Office, Federal Office of Scientific, Technical and Cultural Affairs. The scientific responsibility is assumed by its authors.

[1] M. C. Cross and P. C. Hohenberg, Rev. Mod. Phys. **65**, 3 (1993).
[2] D. Ruelle, in *New Perspectives in Turbulence*, edited by L. Sirovich (Springer-Verlag, New York, 1991).
[3] M. R. E. Proctor and C. A. Jones, J. Fluid Mech. **188**, 301 (1988).
[4] K. A. Julien, Nonlinearity **7**, 1655 (1994).
[5] A. De Wit, G. Dewel, and P. Borckmans, Phys. Rev. E **48**, 6 (1993).
[6] E. Knobloch, Phys. Rev. A **34**, 1538 (1986).
[7] W. Schöpf and W. Zimmermann, Phys. Rev. E **47**, 3 (1993).
[8] K. Fujimura and Y. Y. Renardy, Physica D **85**, 25 (1995).
[9] Ch. Normand, Y. Pomeau, and M. G. Velarde, Rev. Mod. Phys. **49**, 581 (1977).
[10] J. Reichenbach and H. Linde, J. Colloid Interface Sci. **84**, 2 (1981).
[11] P. C. Dauby, G. Lebon, P. Colinet, and J. C. Legros, Q. J. Mech. Appl. Math. **46**, 683 (1993).
[12] L. M. Pismen and A. A. Nepomnyashchy, Europhys. Lett. **24**, 6 (1993).
[13] P. Manneville, *Dissipative Structures and Weak Turbulence* (Academic, New York, 1990).
[14] M. Bestehorn, Phys. Rev. E **48**, 5 (1993).
[15] P. Colinet, J. C. Legros, Y. Kamotani, P. C. Dauby, and G. Lebon, Phys. Rev. E **52**, 3 (1995).
[16] J. K. Platten and J. C. Legros, *Convection in Liquids* (Springer-Verlag, Berlin, 1984).
[17] Ph. Géoris, M. Hennenberg, I. B. Simanovskii, A. Nepomnyashchy, I. I. Wertgeim, and J. C. Legros, Phys. Fluids A **5**, 7 (1993).
[18] P. Colinet and J. C. Legros, Phys. Fluids **6**, 8 (1994).
[19] J. Bragard and G. Lebon, Europhys. Lett. **21**, 8 (1993).

[20] D. V. Lyubimov and M. A. Zaks, Physica D **9**, 52 (1983).
[21] A. Arneodo, P. Coullet, and C. Tresser, Phys. Lett. A **81**, 197 (1981).
[22] M. A. Zaks, Phys. Lett. A **175**, 193 (1993).
[23] Y. Kuramoto and S. Koga, Phys. Lett. A **92**, 1 (1982).
[24] A. S. Pikovsky, M. A. Zaks, U. Feudel, and J. Kurths, Phys. Rev. E **52**, 1 (1995).
[25] S. Rosenblat, G. M. Homsy, and S. H. Davis, J. Fluid Mech. **120**, 91 (1982).
[26] S. H. Davis, Ann. Rev. Fluid Mech. **19**, 403 (1987).